August 1985 LRP 274/85

LASER/ION BEAM DIAGNOSTICS FOR POTENTIAL AND MAGNETIC FIELD MEASUREMENTS IN PLASMAS

R.A. Stern*
Visiting Professor
Centre de Recherches en Physique des Plasmas

LASER/ION BEAM DIAGNOSTICS FOR POTENTIAL AND MAGNETIC FIELD MEASUREMENTS IN PLASMAS

R.A. Stern*
Visiting Professor

Centre de Recherches en Physique des Plasmas
Association Euratom - Confédération Suisse
Ecole Polytechnique Fédérale de Lausanne
21, av. des Bains - 1007 Lausanne / Switzerland

*Permanent address: University of Colorado, Boulder, USA

Work supported by the Fonds National Suisse de la Recherche Scientifique, and by the National Foundation under Grants PHY-8312489 and INT 8405076.

Abstract

Selected initiatives to develop sensors of the local fields, based on extensions of laser-induced fluorescence techniques, are described at both the fundamental and applied levels. In these methods, an ionic or atomic beam is injected into the plasma, and properties of the injected particles which respond to the fields are diagnosed remotely using resonance fluorescence. Approaches discussed include the use of optical pumping ("tagging"); Stark and Zeeman effect methods; and line-narrowing techniques, such as two-photon Doppler-free schemes. Illustrations from recent and unpublished data are presented. Essential problems in data interpretation, such as the interrelationship between Stark and Zeeman effects due to the test particle motion across the fields, are discussed.

1. INTRODUCTION

Plasma physics and fusion have traditionally been swift to exploit new technologies which could serve as diagnostics of plasma properties and processes. Hot ionized gases are easily disturbed by material probes, and also constitute an environment hostile to solid matter [1]. A modern, minimal-probe approach to plasma diagnostics makes use of tuneable lasers to excite quantum transitions in atomic or ionic test species within the plasma, obtaining information on particle densities, temperatures and velocity distributions, and measuring mass transport and fluctuations down to the kinetic scale [2]. To complete the description of the plasma state and processes, which involve field-particle interactions, the detailed structure of electric and magnetic fields in the plasma is required. This review reports on a selected number of recent initiatives to develop sensors of the local fields, based on variations of the tuneable laser/test species technique.

The methods described here are based on the injection into the plasma of an atomic or ionic beam, whose properties will respond to the local field values: together with the remote sensing of these properties using laser-induced fluorescence (LIF). The particle and laser beams can generally be kept sufficiently tenuous to avoid perturbing the plasma. Beam launching and detection are remote, hence suitable for complex plasma devices. Space and time resolution on the scale of 1 mm and tens of nanoseconds are attainable. The basic principles common to these methods are laid out in Section II. Section III describes a variety of approaches. Section IV reports on sub-Doppler techniques. Factors essential to the attainment of adequate signals and their unfolding into useful data are discussed throughout.

II. PRINCIPLES

Because plasmas contain free charged particles, which can group themselves into local sources of net charge and current, electric and magnetic fields within a plasma cannot be evaluated from measurements

of field values outside the plasma. That is, the dielectric or magnetic properties of the plasma are generally complicated functions of the density, temperature, electric and magnetic fields, so that extrapolation from a boundary or initial value is not feasible. Instead, local sensing is required. This is carried out by using test particles in two modes : i. ions, whose space-time trajectory will respond to the Lorentz force by virtue of their charge/mass ratio, and ii. atoms or ions, whose a quantum schemes become altered by the Stark and Zeeman effects. In either case, detection is via a search laser beam which couples strongly to the test particles. Figure 1 is a typical experimental schematic. The interaction is strongest when the laser wavelength λ is tuned to resonance with an allowed (dipole) quantum transition characteristic of the test particle species. A few essentials of LIF techniques will be sketched out below.

A. Laser Induced Fluorescence

The simplest scheme is a quantum interaction involving 2 photons (an incident or absorbed, and an emitted photon), with an atomic species (ion or atom) which can exist in several optically-connected quantum states. These are denoted g ("ground" or initial state), e (excited) and m (final states). The population density n_g of the ground state is introduced into the plasma in reasonably large quantity (see below): a ground or metastable level is best. The transition e-g occurs about a center wavelength λ_g, and has the typical Lorentzian spectral shape $I(\lambda) = \gamma^2 : [4(\lambda-\lambda_g)^2 + \gamma^2]$, a symmetric function of λ centered on λ_g. Here γ represents the intrinsic linewidth (full width at half amplitude) of the transition. An essential feature is that $I(\lambda)$ generally behaves as a very narrow resonance, with γ/λ_g of order 10^{-6} or smaller. This constitutes an ultimate limit on the sensitivity of the techniques described here.

When a laser beam tuned to λ is focused onto the test particles, absorption of laser photons by the particles takes place at a rate proportional to the laser power and to the particle density. The intersection of laser test beam and optical viewing axes defines the center of the diagnosed volume. The relative densities of the states g, e and m are altered by, and evolve as a result of laser

irradiation: in the simplest case (e.g. low laser intensity), a set of rate equations for the densities n_g, n_e and n_m of the various levels can be realistically used. This coupled system involves the laser power P, the particle velocity v, as well as quantum factors, as parameters [3]. Some details of the dynamics will be given below: at this stage we note that the underlying processes are 1. laser-induced depopulation of g, at a rate $P\sigma I(\lambda)g_1 n_g$, where g_1 is a statistical weight and σ is a cross-section; 2. laser-induced depopulation of e, with the rate $P\sigma I(\lambda)g_2 n_e$; 3. spontaneous decay of e, with rates n_e/τ_1 and n_e/τ_2 for the two channel $e \rightarrow g$ and $e \rightarrow m$ respectively. Here τ_1 and τ_2 represent "partial" lifetimes. The last process occurs via the emission of photons at characteristic wavelengths λ_g and λ_m, respectively; i.e. a radiative signature of the process at a wavelength $\lambda_m \neq \lambda_g$ (the laser wavelength) is available.

The cross-section σ is of order $\lambda^2/2\pi \approx 10^{-10}$ cm^2 in the visible, the largest atomic cross-section. As a result, high laser power is not needed. For instance, a 10 mW beam at λ_g (i.e. reasonably narrow in spectrum) focused down to 1 mm^2 corresponds to a flux of 2×10^{18} photons/cm^2-sec (in the visible, ~3 eV photons). Multiplying this by the cross-section we obtain an excitation rate of order 10^8 sec^{-1}. This is close to the reciprocal of the lifetime of excited states (10 nsec in typical cases), and therefore could cause saturation in a two-level system, i.e. when decays $e \rightarrow g$ dominate. It also indicates that, since each excitation is followed by the emission of a photon, the test particles reradiate - in this case - at the rate of 2×10^8 photons/second per g-state particle. Considering that detectors can have intrinsic noise ("dark" current) of order 1 photon/sec, it follows that LIF has the potential for fine-grained diagnostics.

B. Beam Velocity and Doppler Effects

The local field values can, in principle, be diagnosed by using in situ test particles which are in equilibrium with the plasma majority species. In practice, this is rendered difficult by the Doppler spread associated with the plasma temperature T. The spread causes the particles to have a random distribution $f(\underline{v},T)$ of kinetic velocities $\underline{v}$. In the coordinate frame of a particle with $\underline{v}$, the wavelength λ of the laser beam in the laboratory frame is shifted to

$$\lambda' \approx \lambda \left(1 + \frac{\underline{k}\cdot\underline{v}}{k_c}\right)$$

to first order in v/c, where $\underline{k}$ is the propagation vector of the laser ($k \equiv 2\pi/\lambda$; $\hat{k} \equiv \underline{k}/k$). Consequently the absorption spectral profile becomes:

$$I(\lambda,\underline{v}) \approx \gamma^2 : \left[4\left(\lambda + \lambda \frac{\hat{k}\cdot\underline{v}}{c} - \lambda_g\right)^2 + \gamma^2\right] . \qquad (1)$$

The center of the resonance is now shifted by

$$(\hat{k}\cdot\underline{v}/c)\lambda = \lambda \frac{v}{c} \cos\theta$$

where θ is the angle between $\underline{k}$ and $\underline{v}$. Since $\underline{v}$ has random orientation, i.e. all possible θ, so that $-1 < \cos\theta < 1$, the plasma particles end up with resonance center wavelength spread over a range of magnitude $2\lambda\ v/c$. The superposition of Doppler-spread resonances causes the macroscopic (observable) absorption profile to become an integral:

$$\bar{I}(\lambda) = \int_{-\infty}^{+\infty} d\underline{v}\ I(\lambda,\underline{v})\ f(\underline{v},T).$$

For the case $f(\underline{v},T) \propto e^{-mv^2/k_BT}$, a Maxwellian distribution, I is the well-known Voigt profile, which has been tabulated for values of the pair of parameters $(\gamma/\lambda,\ k_BT/mc^2)$[4]. Without recourse to such computations, however, one can estimate from eq. (1) that, if v_{th} is the most probable "thermal" speed of the particles, the resonance broadens from its original value γ/λ_g to roughly $2v_{th}/c$, (when $\gamma/\lambda_g \ll v_{th}/c$). Since even a room-temperature atom has $v_{th}/c \approx 10^{-6}$, it follows that Doppler broadened profiles dominate the absorption, and thus decrease very strongly the precision with which local field values can be measured using spectral techniques.

This problem can be reduced appreciably by introducing the test particles into the plasma as a high-velocity beam [5]. If an assembly of particles with temperature T and most probable thermal speed v_{th} in the rest frame is set into motion without increase in T, and becomes a beam with central velocity $v_B \gg v_{th}$, the particles no longer have an isotropic distribution of kinetic velocity directions. Instead, the velocity vectors are aligned with v_B within a narrow cone of angle $\eta = (v_{th}/v_B) \ll 1$. The Doppler spread due to the

the random orientation of kinetic velocity vectors is thereby decreased. For a laser beam oriented at an angle θ_0 to $\underline{v}_B$, the possible range of angles θ between beam axis and all particle velocity vectors becomes ($\theta \lessgtr \theta_0 \pm \eta$). The Doppler term in the spectral shape now can be expanded:

$$\frac{\hat{k}}{c} \cdot \underline{v} \rightarrow \frac{v_B}{c} \cos\theta \simeq \frac{v_B}{c} (\cos\theta_0 - \eta^2 \cos\theta_0 - \eta \sin\theta_0) \qquad (2)$$

to second order in η. Now η only is random, within its small range 0 to v_{th}/v_B. We see by comparing eqs. (1) and (2) that the beam introduces i. a Doppler shift of magnitude $\lambda\ v_B/c\ \cos\theta_0$ as expected, with a peak value of $\lambda\ v_B/c$ for $\theta_0 = 0$, when the laser is in line with the particle beam; and ii. a Doppler velocity spread of minimum magnitude $v_B/c\ \lambda\eta^2 = \lambda v^2_{th}/v_B c$ (for $\theta_0 \simeq 0$).

The latter is smaller by the ratio v_{th}/v_B than the spread in a stationary medium. Note that the beam v_{th} can be much smaller than the plasma thermal velocity to start with, and remains small if beam-plasma collisions are minimized. Consequently the advantages of narrow resonance are retained by the injection of fast test-particle beams. For instance, a 10 keV beam with 10 eV temperature and $v_{th}/v_B \approx 3\times10^{-2}$ has a Doppler spread of 5×10^{-3} Å, or = 0.02 cm^{-1}, so $\gamma/\lambda g \approx 10^{-6}$ in the visible, equivalent to a room-temperature test particle.

C. Detection and Discrimination

The resonant interaction between laser and test particles causes fluorescence at λ_g and λ_m, which are picked up remotely and serve as the primary sensing signal. The fluorescence at λ_m is spectrally distinct from the laser wavelength $\lambda \approx \lambda_g$, and therefore can be distinguished from light "elastically" scattered (i.e. with little or no frequency shift) from the laser on dust particles, interior walls or optic surfaces. The fluorescence is emitted into 4π steradians, so that remote sensing using finite f-number optics leads to the loss of considerable signal. For instance, a f=2 optical system picks up only 2% of the total fluorescence; and this fraction scales as f^{-2}. A first concern therefore is that the number of signal photons reaching the detectors in a signal event be sufficiently large for detection.

This sets limits on the minimum beam currents. These are simply obtained. Let J be the beam current density in Amperes/cm^2 for an ion beam with a beam velocity v_B, a test volume V, and an optical collection efficiency ε. Then writing $n_g v_B = J$, where n_g is the density of test particles in the beam, the number of signal photons available in a single signal event is

$$\varepsilon n_g V \approx \frac{\varepsilon V J}{v_B} \times \frac{6 \times 10^{18}}{Z} .$$

For instance for $v_B = 10^8$ cm/sec, Z = 1, V = 1 mm^3 and $\varepsilon = 10^{-3}$, engV = 6 x 10^4 J photons. We compare this to the "dark current" of a fast photomultiplier (PMT), say 1 nA or 60 photoelectrons in 10 nsec, the typical duration of a fluorescence signal pulse (the lifetime of the e-state). Recalling that the over-all gain factor, from signal photons to signal photoelectrons, is of order 10^5 including optical losses and quantum efficiency, it follows that acceptable signal may be obtained with microamperes of beam current. This appears reasonable, even taking into account the fact that ion sources emit only a small fraction of ions in the desired g-state if g is not a true ground state, and that some velocity selection will be needed to decrease angular spread.

A more severe restriction on signal/noise usually comes from the radiation reaching the detector from the background plasma, independently of laser and particle beam. The detection system normally collects radiation from a double-conical volume with apex in the test volume [6]. The LIF signal however comes only from the relatively small region of overlap between the cone apex laser and particle beams. The background volume, i.e. the rest of the double-cone, can be much larger, and therefore will contribute appreciable radiation which constitutes noise input to the detector. Each case must be judged on its own merits, but an evident advantage of the laser/ion beam techniques appears here, in comparison with in situ techniques in which one of the species of the background plasma is used as the g-state. First, a test species can be selected for which λ_g lies in a wavelength region in which the plasma is relatively dark. Second, the laser and viewing optics geometry can be adjusted to optimize wavelength discrimination. For instance, let the laser and optics axes be normal to

each other to optimize isolation (reduce "elastic" scatter) and the particle beam axis tangent to their intersection. The absorption and emission profiles now appear Doppler shifted in opposite directions for the laser and detection optics, respectively. For instance a beam with $v_B = 10^8$ cm/sec and λ_g at 5,000 Å will absorb and emit λ shifted by 12 Å away from the center (wavelength of stationary particles). These shifts are sizeable in comparison with quality filter widths (2Å), and of course very large when compared with dispersive instrument resolution (0.1 Å for a 1-meter monochromator). That is, the beam technique provides for superior discrimination against its own species line radiation from the background. Further, the Doppler tuning range available for both laser and detection, enables the diagnostic to be steered away from perturbing coincidences, such as the overlap of molecular Hydrogen emission and the D1 line of BaII at 4934 Å.

D. Interrelation of Electric and Magnetic Fields

A fundamental law which must be applied when diagnosing fields through the use of fast particle beams is the interdependence between electric and magnetic fields, and the velocity of the inertial frame in which they are measured. What we seek is the values of the fields $\underline{E}$, $\underline{B}$ in the laboratory (stationary) frame. In the coordinate frame of a particle moving with velocity $\underline{v}$ however the fields have the values $\underline{E}'$, $\underline{B}'$ are given by the Lorentz transformation [7]:

$$\underline{E}' = (\underline{E} + \underline{v}/c \times \underline{B}); \quad \underline{B}' = (\underline{B} - \underline{v}/c \times \underline{E}) \qquad (3)$$

to lowest order in v/c. That is, there are motional components in the field values sensed by the particles. These must be taken into account.

An important case when these corrections are essential occurs in magnetized plasma, where the confining B can be large but the local electric field strength E of the nearly-neutral plasma is low, and the Stark broadening due to the collisions with charged particles is

negligible. A motional Stark effect will nevertheless occur, when the particle beam velocity has an appreciable component normal to B. This is seen by reference to eq. (3). The motional correction has the magnitude:

$$|\underline{E}'-\underline{E}| = \frac{v}{c} \times 300\ B\ (\text{Gauss})\ ;\ \underline{E}\ \text{in V/cm} \qquad (4)$$

or $\Delta E = 1$ V/cm for $v = 10^8$ cm/sec across a 1 Gauss magnetic field. The slow plasma ions, moving dominantly along $\underline{B}$, are not strongly influenced by this effect. The fast test particles however experience the Lorentz-transformed field, so that it is necessary to know both $\underline{E}'$ and $\underline{B}'$ as well as $\underline{v}$ in order to unfold the laboratory field values, even if only $\underline{E}$ and $\underline{B}$ are sought.

It is easiest to evaluate the magnitude of the motional Stark effect for hydrogenic atoms or ions [8]. In the presence of an electric field E, the quantum state energies are lowered by $3/2\ n(k_1-k_2)\ e\ E\ a$, where n is the principal and k_1, k_2 are parabolic quantum numbers, and a is the Bohr radius (the coefficient of e E is simply the matrix element $\langle nkm|z|nkm\rangle$ along the z-axis defined by E). This causes Stark splitting of spectral lines into components separated by

$$\nu = \frac{3}{2}\frac{eEa}{2\pi\hbar c}\, n\Delta k \simeq 0.0642\ n\Delta k\ E\ (\text{KV/cm})\ ;\ \nu\ \text{in cm}^{-1} \qquad (5)$$

where the energy is expressed in wavenumbers, $hc\nu = 3/2\ n\Delta k\ e\ E\ a$. Typically for high quantum numbers, e.g. $n\Delta k = 15$, ν is 1 cm^{-1}, or 0.25 Å in the visible for E = 1 KV/cm, i.e. a 10^8 cm/sec beam across B=1 KGauss. This exceeds largely the residual Doppler spread of room-temperature particles evaluated above.

To illustrate additional complications introduced by this effect, one compares the Stark splitting due to motion across B, to the Zeeman splitting caused by B in the absence of motion. The Zeeman unit energy change in quantum levels is $(e\hbar/2m_e c)H$, where H is the field and its coefficient is the Bohr magnetron. This causes displacement between

components with a wavenumber shift given by:

$$\sigma = \frac{e\hbar}{2m_e hc^2}\, mgH \simeq 0.0467\ mgH\ (\text{KGauss})\ ;\ \sigma \text{ in } cm^{-1} \qquad (6)$$

where m and g are the magnetic quantum number and the Landé g-factor, respectively. The ratio of Stark to Zeeman shifts is

$$\nu/\sigma = 3\,\frac{n\Delta k}{mg}\left(\frac{m_e ca}{\hbar}\right)\frac{E}{H} \rightarrow \frac{3}{\alpha}\frac{E}{H}\frac{n\Delta k}{mg} \simeq 412\,\frac{E}{H}\ (\text{statvolt/cm}\cdot\text{Gauss})\ \frac{n\Delta k}{mg}$$

$$\simeq 1.37\ \frac{n\Delta k}{mg}\frac{E(V/cm)}{H(\text{Gauss})}\ ,\ \text{where } \alpha = e^2/\hbar c = (m_e ca)^{-1} \text{ is the fine-}$$

structure constant.

When E is entirely due to the motional effect, we have:

$$\nu/\sigma \simeq 412\,\frac{n\Delta k}{mg}\,\frac{v}{c} \qquad (7)$$

using the formulae above, eqs. (4,5 & 6). Thus, for a test particle such as HeII at 10 keV, $\nu/\sigma = 0.34\ n\Delta k/mg$ where the He mass has been used. This ratio can be much larger than unity because of the wide range of possible n and Δk in the numerator relative to m,g. In such cases the test particle spectral structure will be dominated by Stark components, even though the laboratory electric field is very low.

In practice, of course, the test particles will experience the superposition of electric and magnetic fields, so that the preceeding formula is to be taken as exact only in the limit, for instance, of very low B. That is, the actual level shifts must be calculated self-consistently. A typical approach which can be followed is that of Isler [9], who calculates the profiles and polarizations of the Balmer-α line, including the Lorentz $\underline{v} \times \underline{B}$ field as well as the Zeeman effect, in a thermal plasma. A more complex study [10] considers the motional field due to fast atoms or ions in the presence of a self-generated magnetic filed caused by laser-plasma interaction, together with the microfield created by charged-particle collisions. In conclusion, the combination of classical and quantum effects involved can be formidable, and requires wide-ranging expertise.

III. TECHNIQUES

A. Time of Flight and its Limitations

Time of flight methods, through simple, have substantial drawbacks. In straight time of flight techniques, an ion source is gated on or off to create short bursts, whose arrival in the test volume is detected and timed by the pulse of fluorescence emitted when the ion burst enters the laser beam illuminating the volume. The local velocity and its changes, reflecting for instance local electric fields, is obtained by creating several adjacent test volumes separated by intervals Δx along the particle trajectory. The delay time Δt of the fluorescence pulses is related to the local velocity by the integral

$$\Delta t_n = \int_x^{x+\Delta x_n} \frac{dx}{v(x)} \approx \frac{\Delta x_n}{v} \text{ if } v \text{ is constant over the interval } \Delta x.$$

Momentum conservation requires a variation $\Delta\phi$ in the electric potential ϕ between two test volumes to cause a change

$$\Delta v \approx \frac{Ze}{m} \frac{\Delta\phi}{\Delta x} \cdot 2\Delta t \; ; \; \Delta t \equiv \frac{1}{2} (\Delta t_1 + \Delta t_2)$$

in the ion velocity (neglecting the Lorentz force for small v/c and low B). The fractional difference in arrival time delay:

$$\frac{\Delta t_1 - \Delta t_2}{\Delta t} = \frac{Ze\Delta\phi}{mv^2} \text{ for small } \Delta v/v$$

is therefore a measure of the potential difference between the test volumes.

The sensitivity evidently decreases with increasing ion beam energy. If the delay pulse time accuracy were infinite, e.g. sharp laser beam intensity profile and monoenergetic ions, the detector resonance time would be the limiting factor. For Z=1 and a 10 keV beam with $v_B = 10^8$ cm/sec, a spatial resolution of 1 cm imposes Δt = 10 nsec. Using a fast sensitive PMT [11], the time response is at most 0.1 nsec, so that the potential resolution is only of order 10^2eV.

For practicality, a test particle can be chosen having a quantum scheme for which the branching of the spontaneous decays from the excited state is dominantly back to the initial (g) state. That is, optical pumping should be minimized. Then the g-state population is not depleted appreciably by each laser "interrogation", and the pulse amplitudes remain large. The separate laser beams can be obtained from a single laser source, and a single detector viewing the entire test region can be used, since the pulses are separated in time.

A major source of uncertainty in this technique is the velocity spread of the ion bursts. Due to their heavy mass, ion bursts cannot be gated as well as electron beams. Consider, for example, a 10 keV ion beam with $v = 10^8$ cm/sec, switched on in a time which must be short in comparison with the transit time of the ions between test volumes spaced 1 cm apart, or 10 nsec. When an ion source is gated on, an energy spread in the extracted particles is introduced by the switching process. Consider a 1% energy spread, i.e. a 5×10^{-3} velocity variation, in our example. If the distance from ion gun to the test region is 100 cm, a spread of 10 nsec in the arrival time of the front edge of the burst is expected. This smearing of the signal pulses occurs over a time scale comparable to the interval between pulses, 10 nsec since the test volumes are 1 cm apart. The unfolding of such signals would require sophisticated detectors, which can map out the actual signal with nsec response or less, followed by signal processing.

B. Tagging

This method of measuring fields through their effect on ion speed, avoids the complications caused by switching ion beams. An ion beam injected across the plasma is allowed to reach steady state, reducing the velocity spread to a minimum. The quantum scheme chosen is the opposite of that which best suits time-of-flight: a level scheme in which the branching rate e-m is highest will be sought, causing strong optical pumping (laser depopulation) of the initial (g) state. Now the equivalent of the timing signal is obtained by switching the laser beam on. Since one deals with light beams at a

center frequency of order 10^{15} Hz, 1 nsec or less switch times are easily obtained. A second laser beam from the same laser source is positioned at a distance Δx from the first. The fluorescence is elicits will have a simple, monotonic time dependence (see below) on top of which the arrival of the optically-pumped (depleted) g-state ion burst can be distinguished as a pulse. This is, evidently, a time-of-flight method in which laser switching has been substituted for particle gating, and can have a number of variants. We illustrate two of these below, for the relatively difficult cases of a low-energy beam, where the details of the velocity spread can be clearly superposed and identified on top of the basic burst timing [12].

These measurements are carried out in BaII plasmas, where the g-state is the $6^2S_{1/2}$ ground level, which can be excited to the e-state $6^2p_{1/2}$ by radiation at 4934 Å, a convenient wavelength. Strong branching to the metastable $5^2D_{3/2}$ level occurs, so that the g-level is quickly depleted. Two laser beams, a pump beam positioned "upstream", and a search beam displaced 2 cm "downstream", intercept a 1-eV streaming BaII plasma moving along a 3 kG magnetic field from the source. Figure 2a shows LIF measurements of the ion distribution function perpendicular and parallel to the magnetic field, documenting the streaming of the ions. The pump beam is chopped into pulses with rise- and fall-times of 0.1 μsec or less. The search beam is on continuously (i.e. was turned on long before the pump). Radiation from laser-induced fluorescence at the search beam test volume is measured. Its intensity I as a function of time is plotted in the bottom traces (d) of Fig. 2. The lower trace shows a monitor output of the pump-laser intensity. As seen, during the first 9 μsecond after the pump beam is switched on, I remains constant. Then it begins to decrease, but with a decay time much slower (~4 μsec) than the fast rise-time of the pump beam. I reaches a stationary minimum roughly 15 μsec after switch-on, and then increases back to its original level, again with a slow rise-time.

This data is unfolded as follows: the mean beam speed, corresponding to the time displacement between the centers of the pump beam pulse and the search beam fluorescence signal, is 2 cm/15 μsec or 1.3

x 10^5 cm/sec. The time variation of I traces out the spread in velocities within this beam. For instance, the fastest particles arriving at first evidently have a speed of 2 cm/9 μsec, or 2.2 x 10 x 10^5 cm/sec.Note that a detailed unfolding of I(t) must take into account the atomic reaction rates within each beam (see below). It is remarkable nevertheless that such detail can be obtained with lasers incident normally to the particle beam, that is without utilizing the Doppler reduction. This normal geometry may be essential in those configurations where, due to instrumental constraints, a collinear laser-particle beam arrangement is excluded.

An alternative scheme uses pump and search lasers having different wavelengths. Now the search laser induces fluorescence on the transition m-e, measuring the m-state density, so that optical pumping out of g and into the m level by the pump laser elicits an increase in the detected fluorescence intensity I. This is illustrated in Figure 2c. Again, the velocity distribution of the ion beam as well as its center speed are unfolded. The scheme is technically more complicated because of the need for two lasers. Its advantage is that one obtains a "bright" instead of a "dark" signal. That is, if the beam consists dominantly of g-state particles, the background intensity I_0 at the search beam test volume is very low prior to the arrival of the ion burst "processed" by the pump pulse. The signal/noise in such a case is clearly much higher than in a "dark" signal scheme [12].

C. Narrow-Band Measurements

The most technically complex scheme, made feasible by the availability of narrow-band, electronically scannable high-power lasers, traces out the details of the particle beam velocity distribution function directly. A single laser beam is needed. The variation in laser-induced fluorescence intensity I from the test volume is measured as a function of the laser wavelength λ. A reference is required to determine the displacement of the center wavelength due to the beam speed. An example is shown in Fig. 2a. Here a narrow-band laser beam tuned to the vicinity of the 4934 Å line is used with the 1 eV BaII beam described and diagnosed above. Spatial localization is obtained by viewing the laser-induced fluorescence at right angles

using high f-number optics. Shown in this figure is the intensity I for both collinear and normal laser beam incidence. These trace out, respectively, the distribution functions $f(v_\parallel)$ and $f(v_\perp)$ of the components of $\underline{v}$ parallel and perpendicular to the magnetic field axis. This diagnostic has an added advantage: the 3-dimensional trajectory of the particle beam, including the effect of the magnetic field, can be obtained since the center value of $f(v_\perp)$ varies from + to - its peak value as the beam particles execute their cyclotron orbits in the plane perpendicular to the magnetic field. Thus, the combination of the two distribution functions gives the most complete description of the trajectory, and hence of both the electric and magnetic fields.

D. Local Flux Measurements

At the opposite pole of complication, the simplest technique uses a single broad-band unscanned laser incident normally on the particle beam. The atomic scheme involving strong optical pumping, with large branching rate $e \to m$, is used. The particle beam is allowed to come to a steady state, ensuring optimum mono-energeticity. The laser beam is switched on in a time short in comparison with the e-state lifetime (5 nsec or longer), and the laser-induced fluorescence measured locally. The intensity I will exhibit a time-dependence of the form illustrated in Figure 2b. It consists of an abrupt rise to a peak value, followed by a monotonic decrease to a steady-state value. This function can be strongly sensitive to the beam velocity, so that the unfolding of the data is relatively straightforward.

To illustrate this, we consider a simplified version of the full rate equations for quantum-state densities. In the test volume, the g-state density n_g satisfies the equation:

$$\frac{\partial}{\partial t} n_g + v \frac{\partial}{\partial x} n_g = - P_1 n_g - \left(P_2 + \frac{1}{\tau_1}\right) n_e \qquad (8)$$

where v is the beam velocity and the terms on the RHS correspond to i. laser depopulation of g, and ii. decay from e to g via both laser

(induced) and spontaneous processes. Strictly, a similar equation for n_e should be added to the system. A detailed analysis of a more realistic model can be found, for instance in Meng and Kunze [13]. For simplicity, however, assume that n_e is proportional to n_g and that v is constant, so that eq. 8 reduces to the elementary form:

$$\frac{\partial}{\partial \hat{t}} n_g + \frac{\partial}{\partial \hat{x}} n_g = -n_g$$

where time is normalized to $t_0=[P_1 + \alpha(P_2 + 1/\tau_1)]^{-1}$, and space is normalized to vt_0; with α the proportionality coefficient between n_e and n_g. Note that the velocity enters into one of these factors only. The general solution has the form

$$n_g = F(\hat{x} - \hat{t})e^{-\hat{t}}$$

where F is any function of $(\hat{x} - \hat{t})$, and is determined by the initial conditions. That is, an exponential decay in space or time occurs, superposed on a plane-wave like solution propagating with the beam speed. While this idealized solution does not admit of every type of initial or boundary conditions, there is for instance a stationary solution with exponential decrease in n_g. Here the optical pumping rate is balanced by the flux of g-state particles entering the test volume. The space integrated intensity I of the stationary state has the value:

$$\frac{I}{I_0} = \frac{vt_0}{L}(1-e^{-L/vt_0})$$

where I_0 is the initial value (at t=0, corresponding to the initial peak in Fig. 2b), and L is the beam diameter. More elaborate calculations, e.g. [13], lead to roughly similar results, in the sense that I has initial steep rise followed by a slower decay. For the BaII example described above, with $v = 1.3 \times 10^5$ cm/sec, L = 1 mm and t_0 ~100 nsec, $I/I_0 = 0.3$, as in the figure. Thus v_B and its changes will be followed by I with sensitivity in the proper range of parameters. The chief drawback of this method is its reliance on a model equation, and the fact that curve-fitting requires that I be measured as a function of t for an appreciable time beyond the initial decay, i.e. for much more than 5 nsec in the best case. This sets limits on time resolution.

IV. SUB-DOPPLER TECHNIQUES

As shown above, the laser/ion beam technique achieves a decrease in Doppler spread by the factor v_{th}/v_B. Progress towards narrower lines and higher sensitivity along this direction is the task of ion "sorcery", a broad field in its own. An independent line of attack is provided by atomic techniques, some of which will be discussed below.

A. Two-Photon Doppler-Free Resonance (TPDF)

The usual LIF process discussed above, involving 2 photons and an atomic system, is in fact only the lowest-order process in the general description of the interaction of light with atomic systems. In practice, all except extremely faint radiation (e.g. light from isolated stars) consists of more than one photon. The next order, two-photon processes, have a smaller cross-section, but laser beams are now well available in a variety of wavelengths at intensities which make detection easily possible. The basic theory of multi-photon processes is described in several publications [14]. We are concerned here with two special aspects: i. the enhancement in cross-section available in the presence of a near-resonant intermediate state, and ii. the possibility of achieving sub-Doppler resolution through the use of counter-propagating laser beams.

In two-photon processes, an atom in state g interacts with two "incident" photons with wave vectors $\underline{k}_1$, $\underline{k}_2$. Let the two laser beams be collinear but counter-propagating. In the coordinate frame of an atom with velocity v the wavenumbers of the two beam are Doppler-shifted to $k_1{}^1 = k_1 - \underline{k}_1 \cdot \underline{v}/c$ and $k_2{}^1 = k_2 + \underline{k}_2 \cdot \underline{v}/c$ respectively, since the directions of the laser propagation vectors k_1 and k_2 are opposite to each other. The sum of the energies of these photons in the moving frame is:

$$\hbar k_1 c + \hbar k_2 c = \hbar c \left[k_1 + k_2 + (\underline{k}_1 - \underline{k}_2) \cdot \underline{v}/c)\right]$$

for $k \cdot v/c \ll k$, i.e. neglecting the relativistic correction.

The essential here is that the energies are scalars, depending on the magnitudes and not the directions of the k's, and therefore add directly. One sees that for the condition $\underline{k}_1 = \underline{k}_2$, i.e. for two collinear counterpropagating laser beams of the same wavelength, the $\underline{v}$-dependent term vanishes. That is, to first order in v/c, the energy of two identical laser photons counter-propagating has the same total value 2hkc in the frame of all particles, irrespective of their velocity.

If the total energy 2hkc is made equal to the energy differences between the state g and a select state e, under appropriate condition a two-photon excitation can take place. This process now occurs with the same probability for all atoms irrespective of their velocity, since 2hkc no longer contains $\underline{v}$. Consequently the laser beam may be made much narrower in wavelength than the Doppler spread of the atoms, and still cause excitation for all the particles. The linewidth for absorption now is determined by factors such as beam divergence (angular spread in $\underline{k}\cdot\underline{v}$), the second-order Doppler term, etc. The width of the laser line itself can be 3×10^{-5} cm^{-1} or less. Thus, using 2-photon resonance, the Stark and Zeeman spectra can be measured without smearing by the first-order Doppler spread.

The cross-section for the normal TPDF resonance is small, but a large enhancement in cross-section occurs in the presence of a near-resonant intermediate state i. That is, an excited level i must be found, whose energy is close to that of one of the two laser beams, i.e. nearly half the energy difference between e and g. A number of additional condition restrict the choices: first, states g and e must have the same parity. The usual selection rules for 1-photon allowed transitions e-i and i-m must be satisfied. With these conditions, much larger cross-sections can be achieved, so that laser intensities of order 1 MW/cm^2 are sufficient to drive such transitions.

Many examples of enhanced two-photon transition schemes in atoms are known. We describe here an ionic system suitable for use in laser-beam diagnostics. The species is NeII, which has a low-lying quartet system forbidden to decay to the doublet ground state. Of these, the state $3s^4P_{5/2}$ is longest lived (~3 μsec): one-photon LIF measurement

in gas-discharge plasmas reveal that the population of this state is large, and increases quadratically with density (i.e. it is produced by electronic collisions with the ground state) [15].

Two levels present are suitable partners in a TPDF scheme. The $3d^4D_{7/2}$ level as e-state lies at an energy 60,006•84 cm^{-1} above the g-state. Both have even parity, so that single-photon electric-dipole transitions between them are forbidden. The scheme is illustrated in Figure 3. Using a single laser, two identical photons at half the energy difference between the states, 30,003•42 cm^{-1} or a wavelength 333•29 nm in vacuum, are required to drive a two-photon transition. This wavelength is available, with sufficient intensity, from pulsed laser facilities. The i-state $3p^4D_{7/2}$, with odd parity, lies at 29,977•86 cm^{-1} above the g-state, and 30,028•98 cm^{-1} below the e-state. Transitions to both are allowed. The energy mismatch between these energies and the photon is therefore about 26 cm^{-1}, less than 0.1%. Note that the mismatch is large in comparison with the Doppler energy spread (less than 0.1 cm^{-1}) due to ion temperature in the background, and is likely to remain so up to temperature of order 100 eV. Consequently one-photon transitions from the g- to the i-state are excluded at the photon energy used here. Hence the usual approximations of multi-photon process theory are applicable.

The e- and i-levels chosen here have large oscillator strengths, 0.15 and 0.41 for the allowed e-i and i-g transitions respectively. Since the two-photon enhanced excitation rate is proportional to the product of these oscillator strengths, and inversely proportional to the square of the mismatch, it is found that this scheme has a higher transition rate than other feasible schemes, bearing in mind limitation such as the availability of intense laser radiation at the required photon wavelength.

The excitation of two-photon transitions is measured by monitoring the light emitted during spontaneous decay of the e-state. Following each laser pulse, which causes an increase in the population of the $3d^4D_{7/2}$ level, the intensity of the line at 303.446 nm, caused by decays from $3d^4D_{7/2}$ to $3p^4P_{5/2}$, undergoes a sudden

increase. The transition is strong (f≈0.6) and occurs at a wavelength shifted by 30 nm from the laser photons.

A test measurement using an excimer-pumped electronically-scanned dye laser with 1.2 GHz bandwidth and a retroflected beam is shown in Fig. 4 [15]. This displays the output of the gated integrator as a function of the wavelength of the dye laser, in the vicinity of the photon energy 30,003•42 cm^{-1} at which 2-photon resonance can occur. As seen, the observed shape consists of a broad base spanning 100 mA, on which a narrower peak of roughly 15 mÅ is superposed. The theoretical expected shape is shown in Fig. 4b. The broad, Gaussian base represents resonance involving two photons travelling in the same direction (two photon interactions from "the same" beam). Its width should ideally correspond to <u>twice</u> the Doppler spread due to ion temperature. The narrow, Lorentzian peak represents the two-photon Doppler-free resonance, induced by one photon from each of the counterpropagating beams. Its width should be determined by the larger of the laser bandwidth, twice the natural width of the two-photon resonance, etc. The area of the narrow peak is in principle twice that of the Doppler-broadened base. These discrepancies between the experimental and theoretical curves have some possible explanations. The incident and reflected beam are, roughly, crescent-shaped, so that their area of overlap could - due to reversal - be only a small fraction of the beam cross-section. Thus the power in the incident beam overlapping the viewed volume might be much larger than that in the counter-propagating beams. The half-width at half-amplitude (HWHA) of the broad base is about 30 mÅ. If this were to represent twice the Doppler width at 333 nm, the ion thermal speed would be about $1 \cdot 4 \times 10^5$ cm sec^{-1}, matching the background ion temperature, about 0.4 eV, measured by 1-photon LIF. The narrow peak HWHA, very roughly 5 mÅ, corresponds to a linewidth of 0.7 GHz, about half the laser bandwidth in this case.

B. TPDF Motional Stark Measurements

An approach which combines the spectral resolution of two-photon

Doppler-free techniques with the inter-relationship between e and B fields is proposed by Weigert, Rebhan and Kunze [17]. They make use precisely of the fact that, with high values of $\underline{v}$, the v x B motional Stark component can be made much larger than the "straight" Zeeman effect. That is, a component of $\underline{B}$ can be picked out and measured accurately by choosing the directions of $\underline{v}$ suitably. Also, the motional Stark shift can be isolated from the Zeeman effect by using a transition which is essentially unaffected by magnetic field. Their candidate is a transition from the neutral Lithium ground state 2^2S, to the state 4^2D, via 2 photons at 546 nm. They estimate that 1-5 MW pulses are needed. The Zeeman energy level shifts in the Paschen-Back limit have the form:

$$\Delta E = (m_L + 2m_S)\ \mu B$$

where μ is the Bohr magnetron, and m_L, m_S are the orbital and spin magnetic quantum numbers respectively. Using π laser polarization (parallel to $\underline{B}$), only the levels with $m_L=0$ are coupled. Since the Stark effect only mixes levels with the same values of m_S, it follows that the Stark shift appears only on transitions which are not Zeeman-shifted. Hence data unfolding would be simplified.

V. CONCLUSIONS

Remote, non-perturbing field diagnostics in plasmas are a new methodology with many possible directions. It is remarkable that the most recent review of plasma diagnostics [18] could describe on-going efforts initiated several years previously, but no data had been generated : whereas one year later a major component of an international symposium on diagnostics could be devoted to LIF [19]. At the present time, the first results are emerging. Logically, steady-state configurations are most amenable to detail, and have produced quantitative information. Pulsed devices, a more complex problem, are currently yielding preliminary data [19]. These concrete achievements are bound to stimulate further interest and applications.

Among the lines to be followed, one can conclude that i. straight time-of-flight is likely to yield only low-resolution values of the

local potential; ii. tagging (optically pumped schemes) on the other hand overcome the difficulties inherent in t-o-f, since they substitute the inertia of light for that of particle beams. Attention must be paid to data unfolding in these systems, if maximum accuracy is to be obtained. For magnetic field, iii. the role of the Zeeman effect as principal tool is challenged by the motional Stark process, which has two built-in multipliers to increase resolution: the quantum numbers, and the particle velocity. It is encouraging that iv. two-photon Doppler-free processes based on "friendly" ion schemes are being developed. These can supplement - and even replace - the beam Doppler reduction approach, eliminating geometrical restrictions and the limitations imposed by ion sources and injection configurations. Finally, we point out that v. a note of caution should be sounded in connection with all experiments involving sizeable background magnetic or electric fields: their motional interrelation can be strong in particle beam schemes, and lead to unexpected results.

FOOTNOTES AND REFERENCES

[1] For instance, in a 1 keV plasma with charge density 10^{14} cm^{-5}, the thermal particle flux alone contributes several KW/cm^2 to the heat load on a material surface in contact with the plasma.

[2] A recent review is given by R.A. Gottscho and T.A. Miller, Pure and Appl. Chem. 56, 1896 (1984).

[3] The evolution of state densities including transit-time effects and its effects on LIF diagnostics has been treated, for some specific cases, in R.A. Stern, Phys. Fluids 21, 1287 (1978), and R.B. Wright, Nucl. Instr. & Meth. 170, 295 (1980).

[4] J.T. Davis and J.M. Vaughan, Astrophys. J. 137, 1302 (1963); D.G. Hammer, Mem. R. Astr. Soc. 70, 1 (1965).

[5] S.L. Kaufman, Optics Comm. 17, 309 (1976).

[6] A.W. DeSilva and G.C. Goldenbaum, Meth. Exp. Physics 9A, Academic Press, New York 1970, p. 111.

[7] J.D. Jackson, "Classical Electrodynamics", John Wiley & Sons, 1962, p. 380.

[8] E.U. Condon and G.H. Shortley, "The Theory of Atomic Spectra", Cambridge 1963, p. 398-402.

[9] R.C. Isler, Phys. Rev. A14, 1015 (1976).

[10] Nguyen Hoe, S. Grumberg, M. Caby, E. Leboucher and G. Goulaud, Phys. Rev. A. 24, 438 (1981).

[11] I. Yamazaki et al, Rev. Sci. Instr. 56, 1187 (1985).

[12] R.A. Stern, D.N. Hill and N. Rynn, Physics Letters 93A, 127 (1983), and private communication; R.A. Stern, Europhysics News 15, 2 (1984).

[13] H.C. Meng and H.-J. Kunze, Phys. Fluids 22, 1082 (1979).

[14] "High-Resolution Laser Spectroscopy", K. Shimoda, Ed., Springer, New York 1976.

[15] P. Kohler, R.A. Stern, B.A. Hammel, M.Q. Tran, B.M. Lamb, P.J. Paris and M.L. Sawley, Trans. Int. Conf. on Plasma Physics, 317 (1984)

[16] P. Kohler, Ph. D. Thesis, Ecole Polytechnique Fédérale de Lausanne

[17] N.J. Wiegart, U. Rebhan and H.J. Kunze, Physics Letters 90A, 190 (1982)

[18] N.C. Luhman, Jr. and W.A. Peebles, Rev. Sci. Instrum. 55, 279 (1984).

[19] 2nd International Symposium on Laser-Aided Plasma Diagnostics, Culham, 10-12 September 1985.

FIGURE CAPTIONS

Fig. 1: Experimental schematic. Typical configuration using laser beam tangent to ion beam trajectory, to reduce Doppler spread.

Fig. 2: Ion velocity measurements via tagging.

a) Velocity distribution measurements using LIF for reference. Horizontal scale: center of parallel and perpendicular distributions corresponds to 1.3×10^5 cm/sec drift velocity for BaII.

b) Single-laser LIF response in optical pumping scheme.

c) Two-laser LIF using "bright" signal scheme.

d) Two-laser LIF using "dark" signal scheme.

Traces b)-d) obtained with laser beam normal to ion streaming direction.

Fig. 3: Quantum scheme for two-photon enhanced resonance in NeII.

Fig. 4: a) Preliminary observation of two-photon Doppler-free enhanced resonance signal in NeII. Horizontal scale: 0.07 Å between extrema of wavelength scan.

b) Theoretically expected shape of a), under ideal conditions.

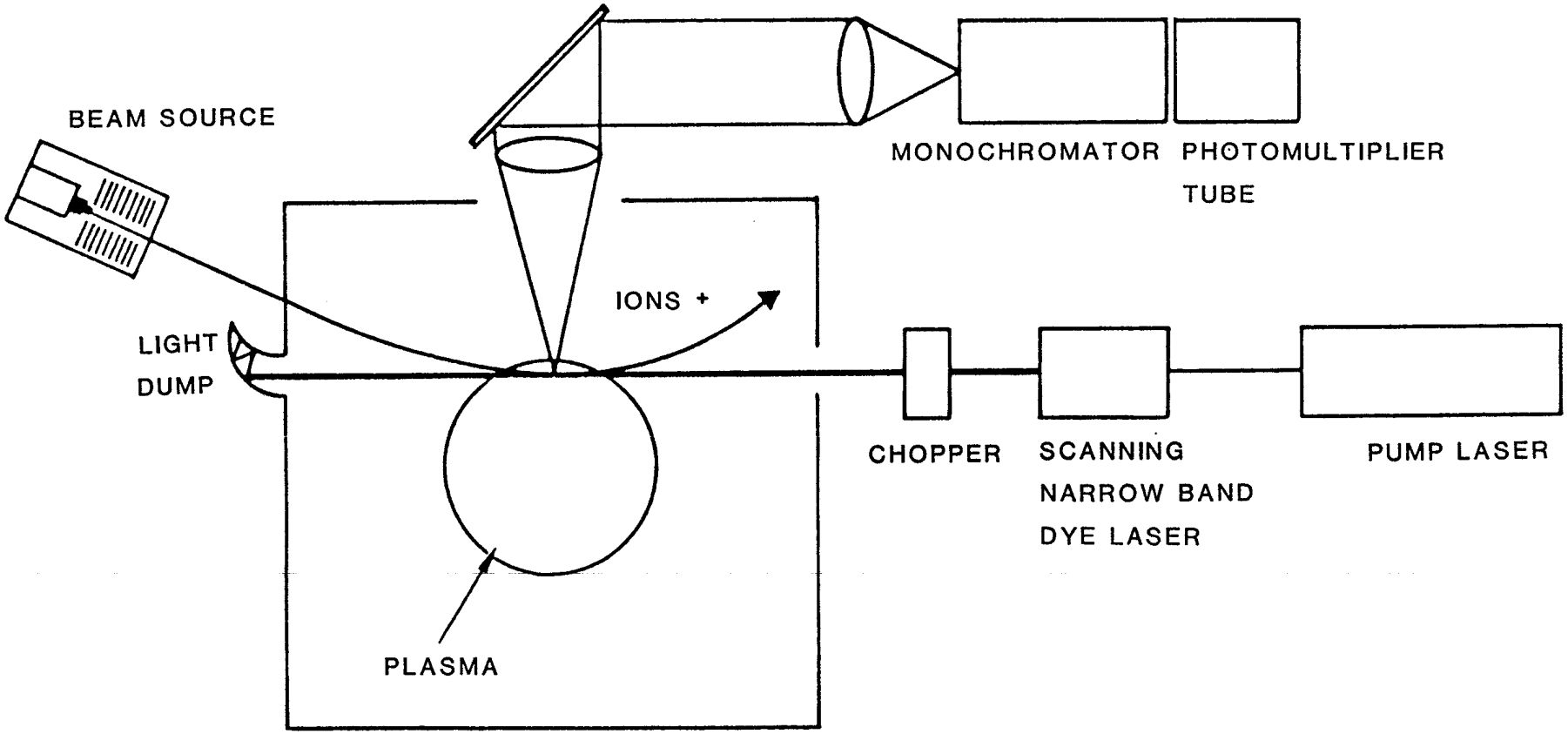
BEAM SOURCE
MONOCHROMATOR
PHOTOMULTIPLIER TUBE
IONS +
LIGHT DUMP
CHOPPER
SCANNING NARROW BAND DYE LASER
PUMP LASER
PLASMA

FIGURE 1

FIGURE 2

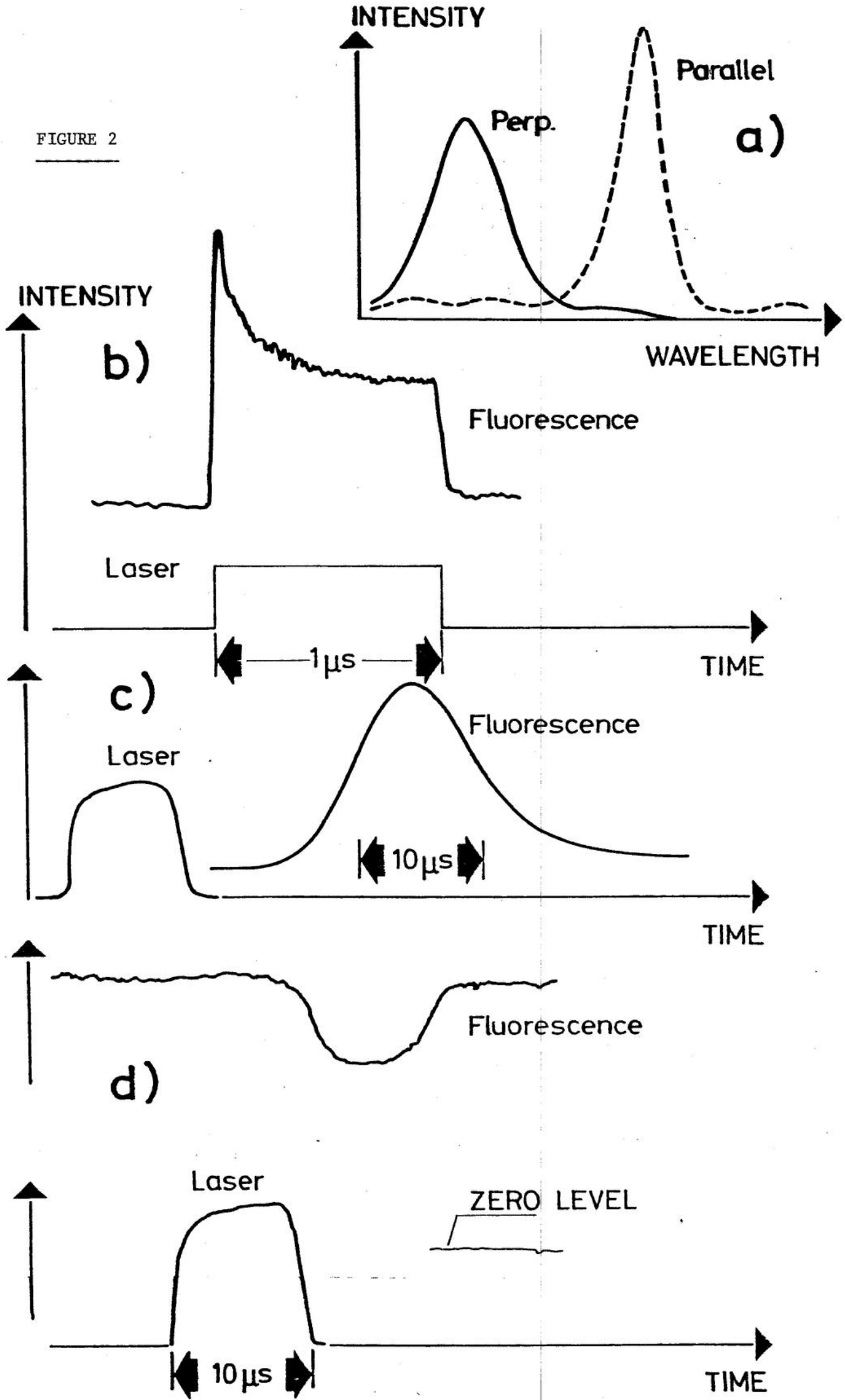
INTENSITY
Parallel
Perp.
a)
WAVELENGTH
INTENSITY
b)
Fluorescence
Laser
1μs
TIME
c)
Fluorescence
Laser
10μs
TIME
Fluorescence
d)
Laser
ZERO LEVEL
10μs
TIME

FIGURE 2

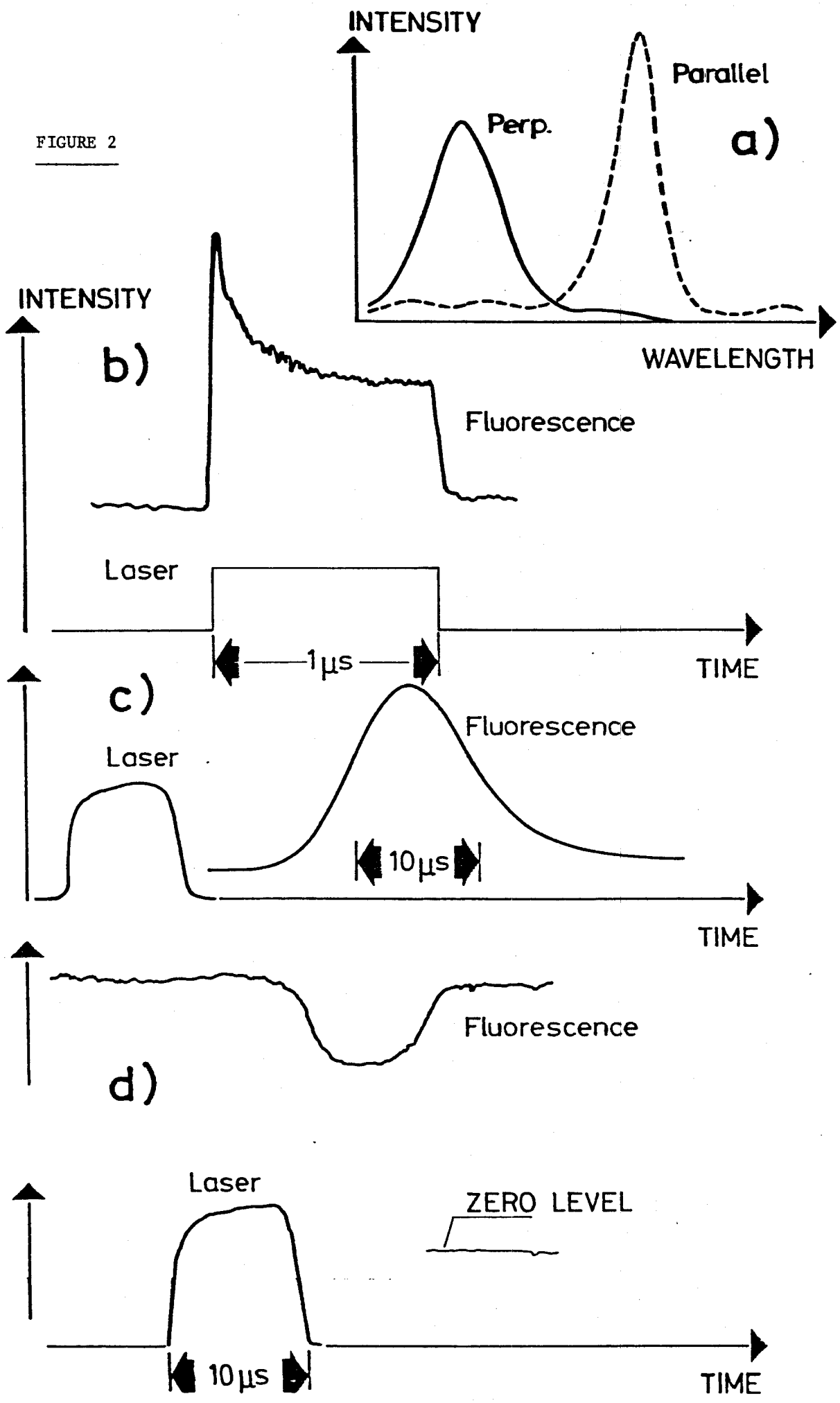
INTENSITY
Parallel
Perp.
a)
WAVELENGTH
INTENSITY
b)
Fluorescence
Laser
1μs
TIME
c)
Fluorescence
Laser
10μs
TIME
Fluorescence
d)
Laser
ZERO LEVEL
10μs
TIME

FIGURE 3

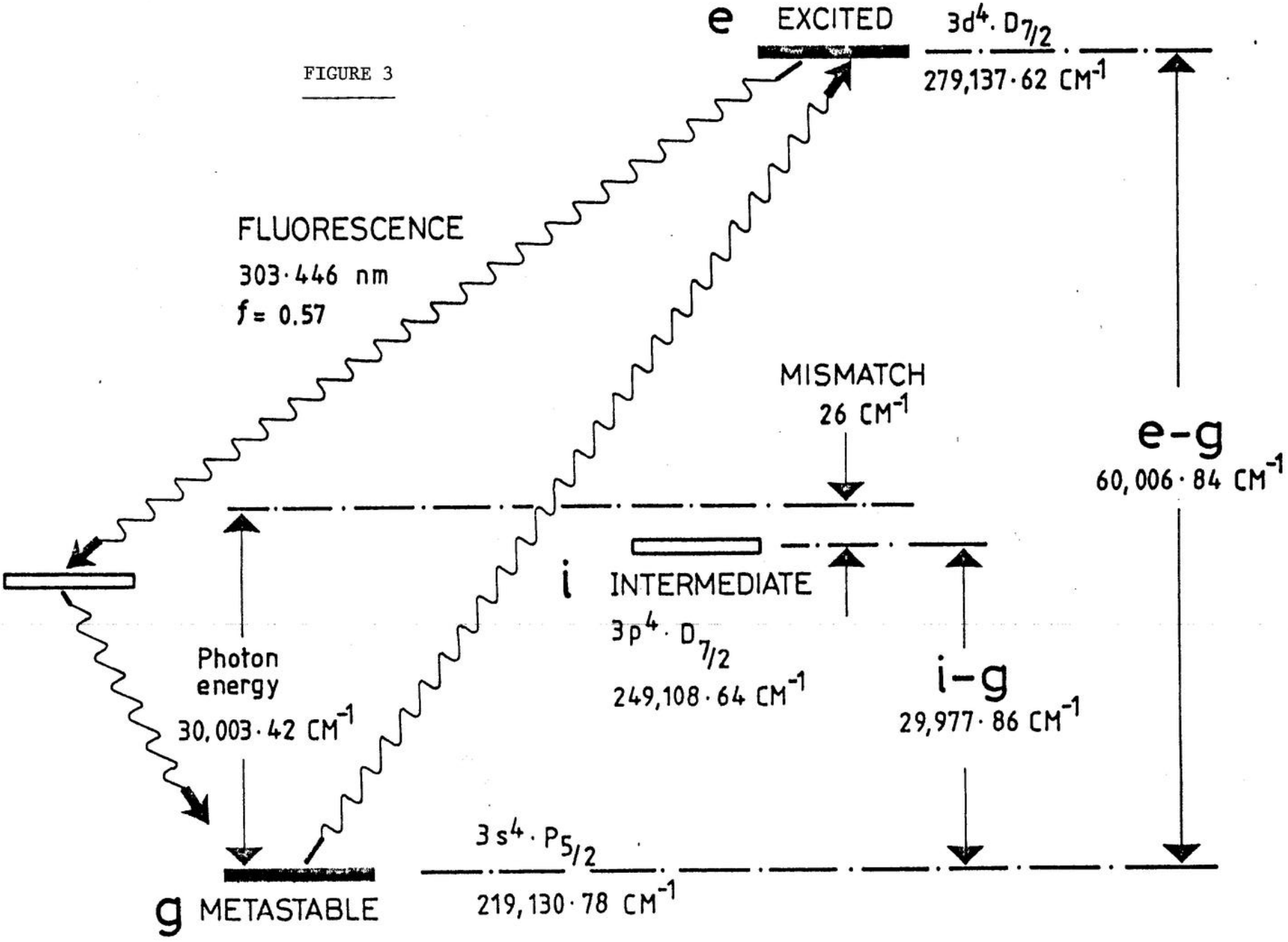
e EXCITED
$3d^4 . D_{7/2}$
279,137·62 CM^{-1}
FLUORESCENCE
303·446 nm
f = 0.57
MISMATCH
26 CM^{-1}
e-g
60,006·84 CM^{-1}
i INTERMEDIATE
$3p^4 . D_{7/2}$
249,108·64 CM^{-1}
Photon energy
30,003·42 CM^{-1}
i-g
29,977·86 CM^{-1}
$3s^4 . P_{5/2}$
219,130·78 CM^{-1}
g METASTABLE

FIGURE 4